Available online at www.sciencedirect.com
ScienceDirect
Geochimica et Cosmochimica Acta 72 (2008) 2491–2509
Geochimica et Cosmochimica Acta
www.elsevier.com/locate/gca

Gypsum as a monitor of the paleo-limnological–hydrological conditions in Lake Lisan and the Dead Sea

A. Torfstein [a,b,*], I. Gavrieli [b], A. Katz [a], Y. Kolodny [a], M. Stein [b]

[a] Institute of Earth Sciences, Givat Ram, The Hebrew University of Jerusalem, Jerusalem 91904, Israel
[b] Geological Survey of Israel, 30 Malkhe Israel St., Jerusalem 95501, Israel

Received 19 March 2007; accepted in revised form 25 February 2008; available online 6 March 2008

Abstract

The isotopic composition and mass balances of sources and sinks of sulfur are used to constrain the limnological–hydrological evolution of the last glacial Lake Lisan (70–14 ka BP) and the Holocene Dead Sea. Lake Lisan deposited large amounts of primary gypsum during discrete episodes of lake level decline. This gypsum, which appears in massive or laminated forms, displays $\delta^{34}S$ values in the range of 14–28‰. In addition, Lake Lisan's deposits (the Lisan Formation) contain thinly laminated and disseminated gypsum as well as native sulfur which display significantly lower $\delta^{34}S$ values (−26 to 1‰ and −20 to −10‰, respectively). The calculated bulk isotopic compositions of sulfur in the sources and sinks of Lake Lisan lacustrine system are similar ($\delta^{34}S \approx 10‰$), indicating that freshwater sulfate was the main source of sulfur to the lake. The large range in $\delta^{34}S$ found within the Lisan Formation (−26 to +28‰) is the result of bacterial sulfate reduction (BSR) within the anoxic lower water body (the monimolimnion) and bottom sediments of the lake.

Precipitation of primary gypsum from the Ca-chloride solution of Lake Lisan is limited by sulfate concentration, which could not exceed ~3000 mg/l. The Upper Gypsum Unit, deposited before ca. 17–15 ka, is the thickest gypsum unit in the section and displays the highest $\delta^{34}S$ values (25–28‰). Yet, our calculations indicate that no more than a third of this Unit could have precipitated directly from the water column. This implies that during the lake level decline that instigated the precipitation of the Upper Gypsum Unit, significant amounts of dissolved sulfate had to reach the lake from external sources. We propose a mechanism that operated during cycles of high-low stands of the lakes that occupied the Dead Sea basin during the late Pleistocene. During high-stand intervals (i.e., Marine Isotopic Stages 2 and 4), lake brine underwent BSR and infiltrated the lake's margins and adjacent strata. As lake level dropped, these brines, carrying ^{34}S-enriched sulfate, were flushed back to the shrinking lake and replenished the water column with sulfate, thereby promoting massive gypsum precipitation.

The Holocene Dead Sea precipitated relatively small amounts of primary gypsum, mainly in the form of thin laminae. $\delta^{34}S$ values of these laminae and disseminated gypsum are relatively constant ($15 \pm 0.7‰$) and are close to present-day lake composition. This reflects the lower supply of freshwater to the lake and the limited BSR activity during the arid Holocene time and possibly during former arid interglacials in the Levant.

1. INTRODUCTION

Modern deposition of evaporites commonly takes place in shallow-water saline lakes such as Lake Magadi (Eugster, 1970) and Lake Chad (Eugster and Maglione, 1979) in Africa, Lake Eyre basin in Australia (Magee et al., 1995), Great Salt Lake in North America (Spencer et al., 1985), and many others. However, the majority of thick evaporite sequences known from geological records precipitated from seawater-derived solutions such as the Mediterranean Messinian (Hsu et al., 1977; Krijgsman et al., 1999), the Permian basins of Texas and the Zechstein in Europe (cf. Anderson et al., 1972; Glennie and Buller, 1983; Warren, 1989; and references therein). These thick sequences

* Corresponding author.
E-mail address: adi.torf@mail.huji.ac.il (A. Torfstein).

0016-7037/$ - see front matter © 2008 Elsevier Ltd. All rights reserved.
doi:10.1016/j.gca.2008.02.015

however, could not have precipitated directly from seawater which are undersaturated with respect to the dominant evaporitic minerals (i.e., gypsum, halite). Thus, massive evaporite deposition is generally explained by the occurrence of repeated cycles of desiccation and re-filling or alternatively, a continuous inflow and evaporation configuration (cf. Hsu et al., 1977; Krijgsman et al., 1999; Warren, 1989). The hypersaline nature of the precipitating solutes, the varying degrees of drawdown required for the precipitation of thick evaporate sequences and the depth of water (i.e., deep- vs. shallow-water) in such ancient water bodies are difficult to estimate and have been widely debated (cf. Warren, 1989; Kendall, 1992; and references therein).

The Dead Sea, which is a unique modern analogue to deep-water evaporite systems, is a hypersaline, Ca-chloride lake that despite extremely high calcium concentrations (~17 g/l) does not support massive gypsum precipitation. This mainly reflects the low sulfate concentration (<0.4 g/l). On the other hand, sediments deposited from Lake Lisan, the late Pleistocene precursor of the Dead Sea, contain thick sequences of gypsum, indicating enhanced supply of sulfate to the lake (Begin et al., 1974; Stein et al., 1997; Torfstein et al., 2005).

In this study we set out to understand the hydrological–limnological conditions that enabled the deposition of primary gypsum in the hypersaline Ca-chloride lacustrine water bodies in the late Quaternary Dead Sea basin. The water bodies represent terminal amplifier lakes whose geochemical and physical characteristics reflect the hydrological-climatic conditions that existed in their large drainage area and therefore provide important information regarding the climatic history of the Levant during the Quaternary (cf. Stein, 2001; Enzel et al., 2003). We focus on the hydrological conditions during the intervals of massive gypsum deposition, which occurred during relatively arid stages and subsequent lake level declines (Stein et al., 1997). We investigate a major cycle of gypsum deposition spanning the transition from Marine Isotopic Stage 2 (MIS2) to MIS1 and use sedimentological and geochemical ($\delta^{34}S$) data to characterize the depositional environment. Exploring the deposition mechanisms of gypsum in the Dead Sea basin water bodies and explaining their connection to the recurring fluctuations between long-term high-stands to long- and short-term low-stands provides strong constraints on the depth of the water and the regional hydrological-climatic regime. In addition, the differences in the limnological–hydrological setting between the last glacial and the Holocene water bodies are discussed.

1.1. Paleo-limnological background

The series of water bodies that existed in the tectonic depressions along the Dead Sea Rift (DSR) during the Quaternary evolved from the ancient (Pliocene?) Sedom Lagoon which derived its chemical constituents from ingressing seawater and interaction with the carbonate wall-rock. Subsequently, DSR brines obtained their unique Ca-chloride composition (Zak, 1967; Starinsky, 1974; Stein et al., 2000, 2002). After the disconnection of the Sedom lagoon from the open sea, the limnological and geochemical history of the now closed and terminal water bodies was controlled by the interaction between the brine and the freshwater input from the drainage area of the Dead Sea basin (Katz et al., 1977; Stein, 2001; Gavrieli and Stein, 2006).

The freshwater influx and the limnological configuration of the lakes (stratified vs. homogeneous water column) reflect the climatic–hydrologic history of the region, which fluctuated during the Quaternary between arid to semiarid conditions (Begin et al., 1974; Bartov et al., 2002, 2003; Prasad et al., 2004; Haase-Schramm et al., 2004) and correlate to global climatic trends, as recorded by oxygen isotopic ratios and other proxies in Greenland ice and deep-sea cores.

During wet stages, lake level rose and water column stratification developed. Long-term stratification required a positive water balance maintained by freshwater influx. Overturn and mixing of the water column occurred when the salinity of the upper water body (the mixolimnion) increased again, which occurred upon a shift to a negative water balance. Changes in the water column configuration and consequent geochemical processes are reflected by the chemical and isotopic composition of the sediments (i.e., Sr/Ca and $^{87}Sr/^{86}Sr$ ratios (Katz et al., 1977; Katz and Kolodny, 1989; Stein et al., 1997) and $\delta^{34}S$ values (Torfstein et al., 2005)).

1.2. Geological background

The Lisan Formation (Fm.), deposited by the Late Pleistocene Lake Lisan (~70 to 14 ka BP; Kaufman, 1971; Haase-Schramm et al., 2004), is exposed along the Dead Sea basin, from the northern Arava valley in the south to the Sea of Galilee in the north (Fig. 1).

The lake was sensitive to hydrological changes in its large drainage area, and its level, which responded to wet and arid episodes within the last glacial interval, fluctuated between ~160 to 370 m below mean sea level (mbsl) (Fig. 2; Bartov et al., 2003). During high stands the lake precipitated sequences of thin (~1 mm) aragonite laminae alternating with silt-sized detrital laminae (this facies is termed alternating- aragonite-detritus ("*aad*") facies; Machlus et al., 2000). While the aragonite precipitated chemically from the lake, the detrital laminae, composed mainly of calcite, quartz, dolomite and clay, are the erosion products from the Dead Sea rift shoulders as well as eolian input from more distant terrains (Neev and Emery, 1967; Begin et al., 1974; Haliva et al., 2003). During low stands, the lake deposited gypsum as the main evaporitic mineral phase.

The main study site in this work is the M1 sedimentary section located on the foothills of the Massada archeological site (Fig. 1). Here, the base of the formation is located at 374 mbsl, overlying the exposed top of the last interglacial Samra Fm. (Waldmann et al., 2007), and is approximately 30 m thick. Additional samples were collected from Perazim Valley, Mt. Yizrach, Nahal Mor, Nahal Mishmar, Bet Ha'arava and Deir Shaman (Fig. 1).

The Massada M1 section consists of three stratigraphic Members (Fig. 2). The Lower Member is 5.6 m thick and consists mainly of *aad* sequences, which are capped by a se-

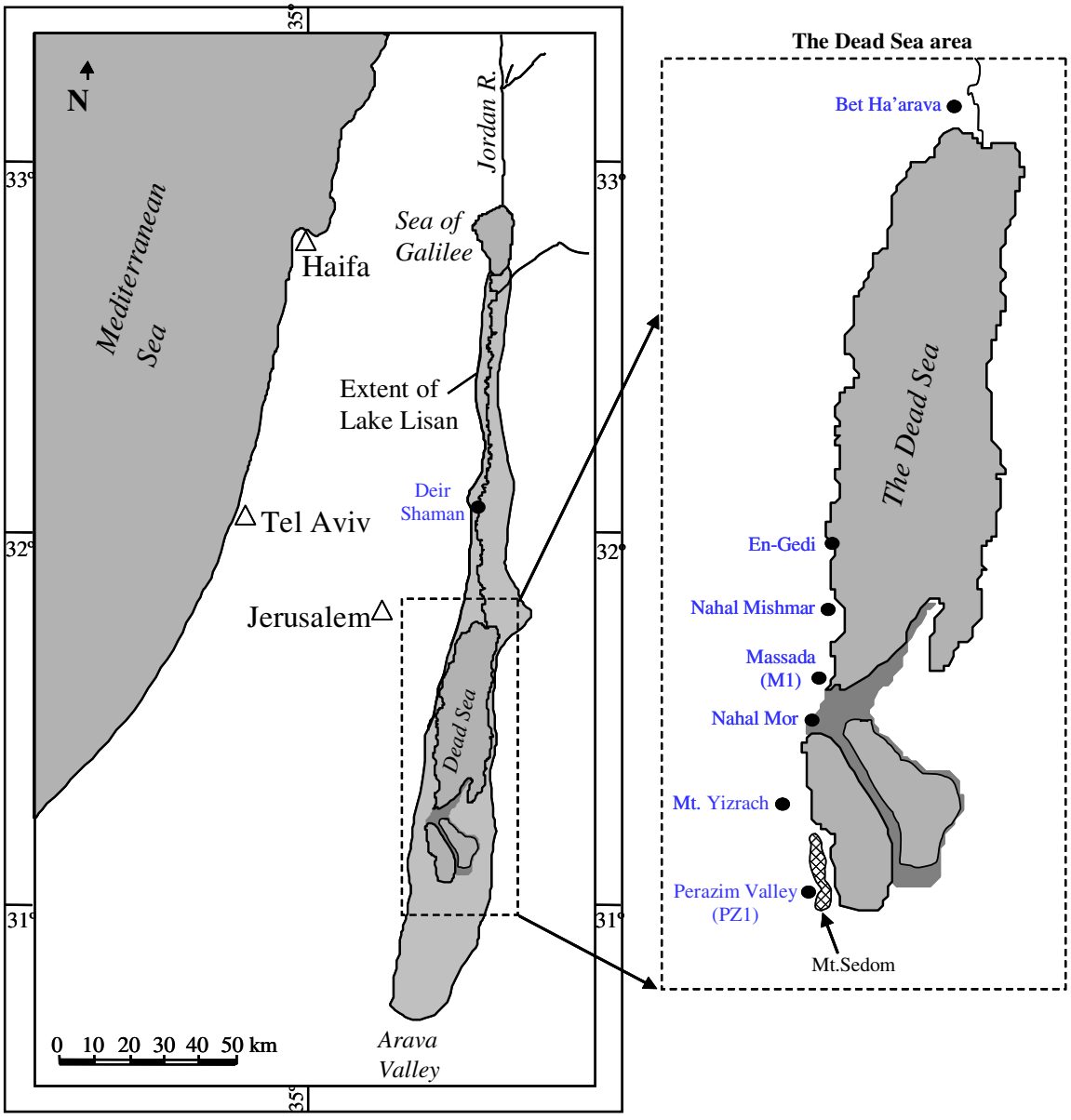

Fig. 1. Location map of sampling sites (marked by black circles) along the Dead Sea Basin. Maximum extent of Lake Lisan is marked in the left panel.

quence containing three gypsum layers. The latter can be correlated over large distances in the Dead Sea basin (Waldmann et al., 2007). The Middle Member is 11.5 m thick and is comprised of abundant clastic beds (sands and silts), which alternate with *aad* packages and some gypsum layers. The Upper Member is 13.5 m thick and consists of a 9 m thick *aad* sequence which is capped by a ~2 m thick sequence of gypsum layers alternating with *aad* bundles. These are overlain by an additional unit of *aad* and gypsum. The transitions from the Lower to Middle and from the Middle to Upper Members coincide with the main Marine Isotopic Stages (MIS) boundaries: 4–3 and 3–2, respectively (Stein, 2001; Bartov et al., 2003; Haase-Schramm et al., 2004).

The Lisan Fm. is overlain by sediments of the Ze'elim Fm. deposited from the Holocene Dead Sea, whose typical levels were ~400 ± 30 mbsl (Bookman (Ken-Tor) et al., 2004; Migowski et al., 2006). The Ze'elim Fm. consists of layered calcitic marls, alternating laminae of aragonite–silty detritus couplets or aragonite–gypsum–silty detritus triplets, and several sand layers (Migowski et al., 2004, 2006). No massive gypsum units were deposited by the Holocene Dead Sea and the overall amount of aragonite is small relative to the Lisan Fm.

1.3. Sulfur in the Dead Sea and Lake Lisan

By definition, Ca-chloride solutions are low in sulfate $\left(\frac{Ca^{2+}}{SO_4^{2-}+HCO_3^-} > 1_{(eq.)}\right)$ (Hardie and Eugster, 1970; Starinsky, 1974; Eugster and Jones, 1979). Indeed, the Ca-chloride water bodies of the DSR are (and were) characterized by

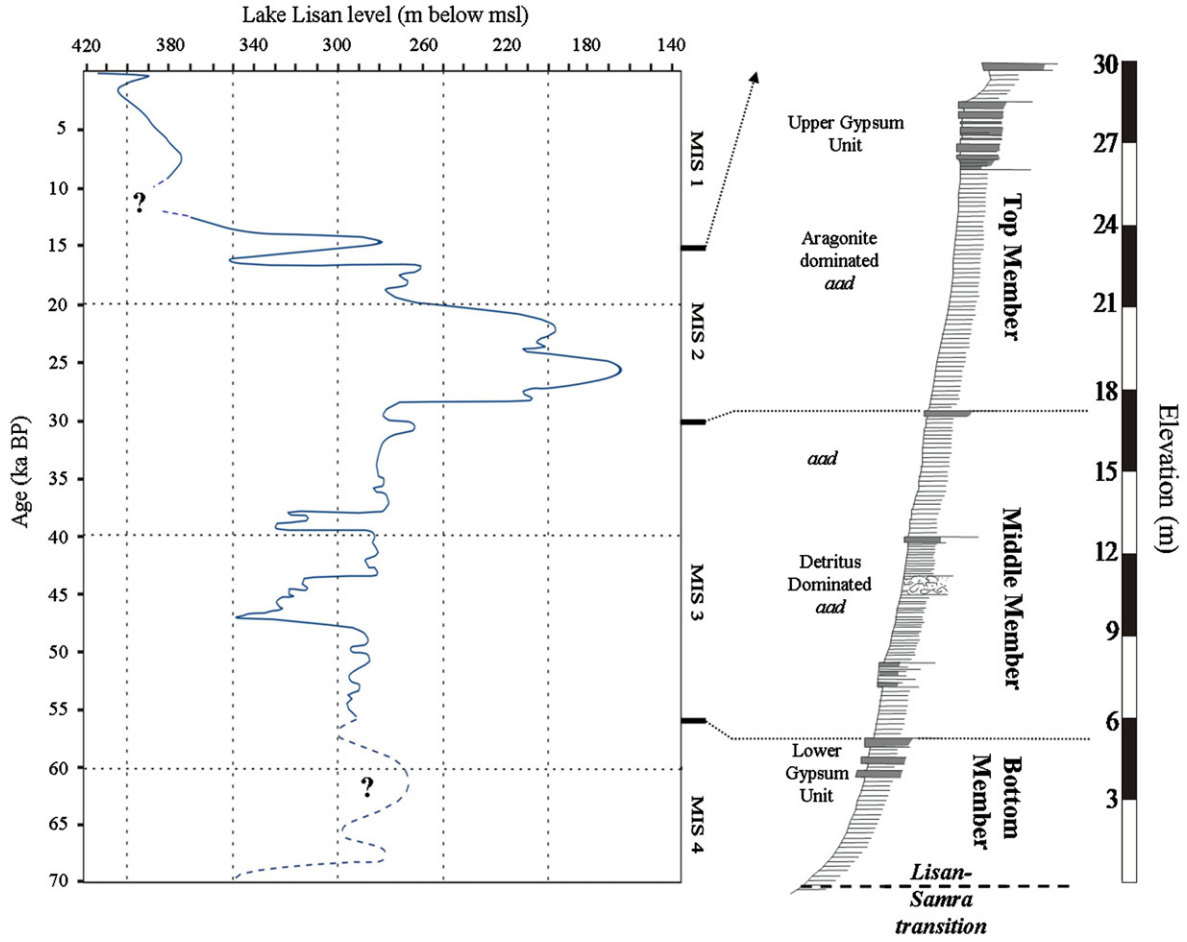

Fig. 2. The Massada sedimentary section correlated to the lake level curve of Lake Lisan. The sedimentary column is comprised of gypsum layers (marked in grey) and alternating aragonite and detritus laminae (*aad* facies marked by thin lines). A "convolute" unit appears at ~11 m (see Bartov et al. (2002) for details). The transitions from the Lower to Middle and from the Middle to Upper Members of the Lisan Formation coincide with the transitions from Marine Isotopic Stages (MIS) 4 to 3 and from 3 to 2, respectively. The lake level curve is modified after Bartov et al. (2003).

relatively low sulfate concentrations (e.g., <400 mg/l in the 20th century Dead Sea, compared to calcium concentration of ~17,000 mg/l; Neev and Emery, 1967). The modern Dead Sea brine is supersaturated with respect to gypsum (Katz et al., 1981) and the residence time of dissolved sulfate in it is relatively short (100–1500 years; Torfstein et al., 2005). Thus, it has been suggested (Stein et al., 1997) that the sulfate dissolved in the DSR lakes is derived mainly from inflowing freshwater.

Based on the analyses of various freshwater sources in the DSR drainage area, the bulk isotopic composition of dissolved sulfate presently discharging into the Dead Sea is estimated to lie within $\delta^{34}S \approx 6$–$14‰$. Since the same water sources were active in the Late Pleistocene too, it can be assumed that this range also represents the isotopic composition of the dissolved sulfate that reached Lake Lisan (Torfstein et al., 2005). However, sulfur occurrences in the Lisan Fm. display a bimodal isotopic composition (<1‰ and >14‰; Figs. 3 and 4; Torfstein et al., 2005), which is inconsistent with direct precipitation of gypsum from the water column. Rather, these compositions imply the occurrence of sulfur isotopic fractionation induced by bacterial sulfate reduction (BSR). This process takes place under anoxic conditions following the simplified reaction:

$$2CH_2O + SO_4^{2-} \Rightarrow 2HCO_3^- + H_2S \quad (1)$$

The anoxic conditions required for BSR could have evolved in the lake's lower water body (the monimolimnion), when the lake was stratified, or within the bottom sediments. The source and type of the organic matter that was oxidized during the BSR is not known although it has been attributed to algal blooms in the diluted mixolimnion (Oren et al., 2004; Kolodny et al., 2005). BSR is typically accompanied by isotopic fractionation whereby preferential reduction of $^{32}SO_4^{2-}$ results in the remaining sulfate anions becoming enriched in ^{34}S (Kaplan and Rittenberg, 1964; Kemp and Thode, 1968; Chambers et al., 1975; Habicht and Canfield, 1996; Canfield, 2001). In the modern Dead Sea and the surrounding saline springs, the isotopic fractionation associated with BSR has been determined to be 25–30‰ (Nissenbaum and Kaplan, 1976; Gavrieli et al., 2001). A similar value was attributed to the Lisan system (Torfstein et al., 2005).

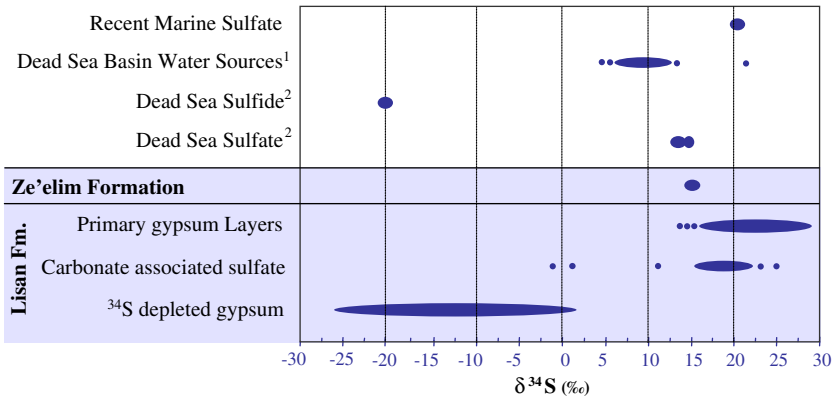

Fig. 3. $\delta^{34}S$ values of the main sulfur occurrences in the Lisan and Ze'elim Formations and in other relevant environments. *Sources:* [1]Data compilation by Torfstein et al. (2005); [2]Nissenbaum and Kaplan (1976).

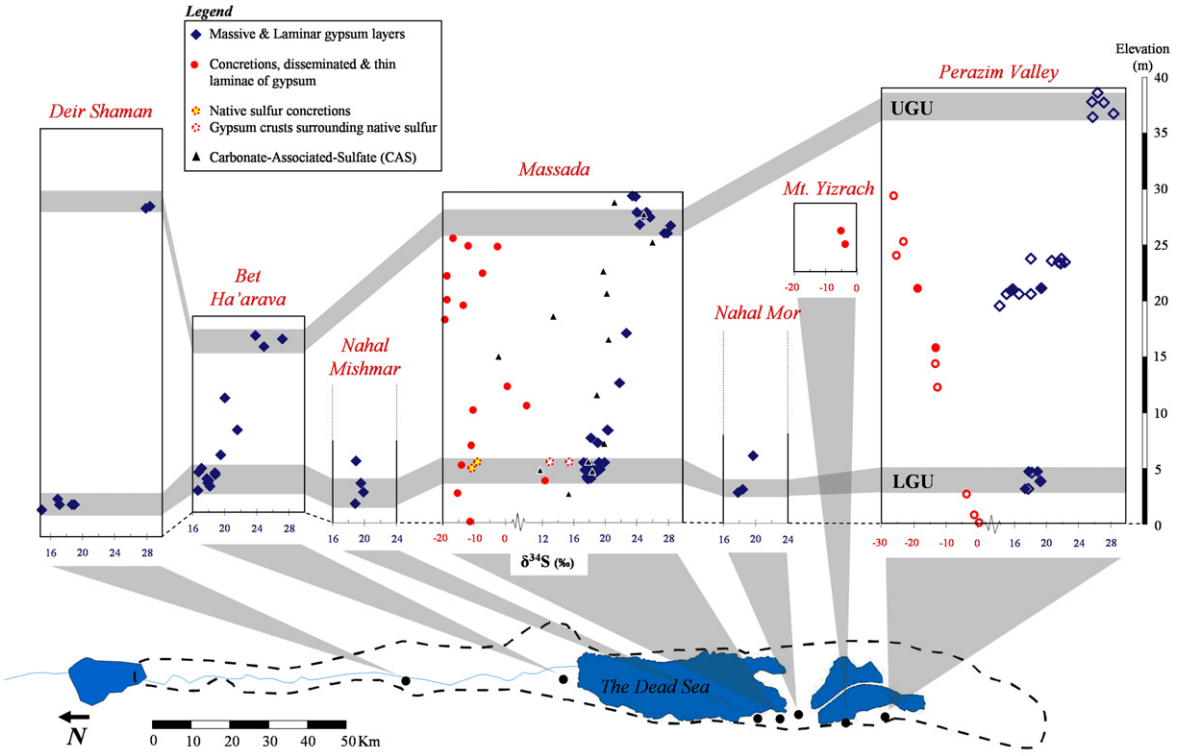

Fig. 4. $\delta^{34}S$ values in the Lisan Fm. from seven sampling sites along the DSR. The thick grey lines emphasize the Lower Gypsum Unit (LGU; bottom) and the Upper Gypsum Unit (UGU; top). Note the lateral homogeneity in $\delta^{34}S$ values in synchronously deposited gypsum layers. Empty symbols in the Perazim Valley section are from Torfstein et al. (2005).

During wet periods, when the lake was stratified and undersaturated with respect to gypsum, dissolved sulfate that entered the lake first accumulated in the mixolimnion. When enough sulfate accumulated in the mixolimnion gypsum saturation was reached and additional sulfate inflow lead to gypsum precipitation. In contrast, intensive BSR in the monimolimnion decreased the sulfate concentration therein, which became under-saturated with respect to gypsum. Any gypsum that precipitated from the mixolimnion and sank through the monimolimnion was thus susceptible to dissolution. Accordingly, inflowing sulfate was transported from the mixolimnion via continuous gypsum precipitation to the monimolimnion where it re-dissolved. Concurrent BSR in the monimolimnion produced residual ^{34}S-enriched sulfate as well as ^{34}S-depleted sulfide which was removed to the sediments. Torfstein et al. (2005) calculated that a steady state value of $\delta^{34}S_{SO_4} \approx 40‰$ was reached in the monimolimnion after several thousands years of meromictic conditions.

Upon a decrease in the freshwater flux into the lake, lake level dropped and the increased salinity (and thus density) of the mixolimnion led to overturn and mixing of the water column and to massive precipitation of gypsum. The isotopic composition of sulfur in this gypsum represents that of the

mixed water body which in turn depends on the relative volumes, dissolved sulfate concentrations and isotopic compositions of sulfate in the two water layers before the overturn.

The ^{34}S-depleted sulfides were most probably removed from the brine through precipitation of Fe-sulfide phases and were buried in the sediments. The high sedimentation rate of Lake Lisan decoupled these phases from the aqueous system soon after deposition. Thus, during water column mixing and oxidation the reduced sulfides were not susceptible to immediate oxidation and therefore were not recycled back into the brine. Sulfide oxidation took place only after the retreat of the lake and sediment exposure. Because sulfide oxidation involves only minor isotopic fractionation (Fry et al., 1986, 1988; Habicht et al., 1998) the original low δ^{34}S values were preserved in the oxidized sulfate which, given the abundance of calcium in the exposed sediments, promptly precipitated and formed disseminated and thin laminae of gypsum. Evidence for the extensive oxidation of the Lisan Fm. sediments was provided by Ron et al. (2006). Based on the magnetic properties of the sediments, they suggested that only negligible fractions of the original reduced phases were preserved. By comparison, they observed that the freshly exposed Holocene Ze'elim Fm. displays a higher content of ferromagnetic Fe-sulfide reduced phases (i.e., greigite).

2. METHODS

2.1. Sampling

Samples, approximately $30 \times 30 \times 30$ cm^3 in size, were collected from several sections along the DSR (Fig. 1). The samples were wrapped in adhesive plastic foils to prevent disintegration of the soft sediments. Gypsum samples from Holocene (Dead Sea) sediments were picked by C. Migowski from a sedimentary core drilled at the En-Gedi shore (a detailed description of the core is given in Migowski et al., 2006).

The gypsum content in two primary gypsum layers in the M1 section was estimated by extracting two duplicates of 30 cm long cores from each layer. The retrieved sediments were grinded and washed in de-ionized water to dissolve the gypsum. The filtered solution was analyzed for sulfate and the results were used to calculate gypsum content. XRD of the insoluble residue was used to verify that no gypsum remained undissolved.

2.2. Chemical analyses

To determine the sulfate content in the different lithological sequences, individual laminae of aragonite, detritus and gypsum, as well as bulk samples, ~5 g each, were scraped with a scalpel knife. Following grinding and homogenization, the mineralogical composition of each sample was determined by XRD. Soluble salts were water-leached from the aragonite and silty-detritus samples (Katz and Kolodny, 1989) and the aragonite was dissolved in 1.2 N HCl. Sulfate concentrations in dissolved aliquots were measured by ICP-AES (Perkin-Elmer Optima 3000) at the Geological Survey of Israel (GSI).

2.3. Isotopic analyses

Gypsum samples were dissolved in de-ionized water, filtered, and the sulfate precipitated as $BaSO_4$. The precipitate was collected on Whatman^{TM} #42 filter paper, thoroughly washed with de-ionized water and burned at 850°C.

At an early phase of the study, samples were analyzed off-line: the $BaSO_4$ was introduced into a vacuum extraction line at the GSI, where SO_2 gas was produced and separated following Coleman and Moore (1978). The SO_2 gas was collected in gas ampoules, and isotopic analyses were performed on a Sira II mass spectrometer at the British Geological Survey ($n = 45$). Additional analyses of $BaSO_4$ were conducted using a TracerMass-Roboprep system (Europa-UK) at the University of Waterloo, Canada ($n = 53$). A Flash EA 1112 series elemental analyzer connected in a continuous flow mode to a Thermo Finnigan Delta^{plus} mass spectrometer (Giessemann et al., 1994) was used for measurements at the University of Arizona, USA ($n = 14$) and at the Hebrew University of Jerusalem, Israel ($n = 8$). Table 1 identifies the laboratory in which each sample was analyzed.

Sulfur isotope compositions are expressed as permil (‰) deviations from the V-CDT standard using the conventional delta notation. The overall analytical reproducibility, including our inter-laboratory calibration, is ±0.4‰ as determined by direct calibration against sulfur isotopic standard NBS-127 (+20.3‰; $n = 70$).

3. RESULTS

3.1. Sulfur occurrences in the Lisan Formation

Sulfur in the Lisan Fm. occurs in several forms (Tables 1–3 and Figs. 3–5):

3.1.1. Primary gypsum layers

Two types of layers, approximately 10–20 cm thick, are identified: *massive fine-crystalline gypsum* with little internal lamination, and *laminar gypsarenite*, exhibiting alternations between gypsum, detritus and sporadic aragonite laminae. Both types display δ^{34}S values of 14–28‰. Two prominent gypsum units, the Lower Gypsum Units (LGU; $\delta^{34}S = 16$–20‰) and the Upper Gypsum Unit (UGU; $\delta^{34}S = 25$–28‰), span over all the studied sites (Fig. 4), where they retain their texture and isotopic composition. The units are comprised of several consecutive gypsum layers, with intermittent *aragonite–silty detritus* (*aad*) sequences. A gradual lateral decrease in thickness of the gypsum layers is observed: their thickness at the northern exposures of the Lisan Fm. (Deir Shaman site; Fig. 1) is approximately half that of the corresponding thickness in the central Dead Sea basin (Massada M1 section; Fig. 5).

3.1.2. Thin gypsarenite laminae, selenite concretions, and disseminated gypsum

These gypsum occurrences are typically associated with detrital laminae of *aragonite–silty detritus* where they distort and offset the neighboring layers. The laminae are ⩽1 mm thick, and have no significant lateral extension.

Table 1
Mineralogical and isotopic ($\delta^{34}S$) compositions of samples collected from the study sites

Site	Sample	Elevation (cm)	Lithological type	Mineralogy	$\delta^{34}S$ (‰)	Lab
Bet Ha'arava	BA 170	1582	Coarsely laminated layer	G + Q	23.9	a
	BA 150	1544	Massive gypsum layer	G	27.4	a
	BA 100	1490	Coarsely laminated layer	G + A	25	a
	BA 80	1034	Coarsely laminated layer		20.2	d
	BA 70	733	Coarsely laminated layer		21.6	d
	BA 60	527	Laminated gypsum layer		19.3	d
	BA 35	344	Laminated gypsum layer	G + Q, A, C	16.9	b
	BA 33	339	Aragonite laminae	A + G, C	17.3	b
	BA 32	331	Laminated gypsum layer	G + A	18.7	b
	BA 31	317	Laminated gypsum layer	G + A, Q	18.7	b
	BA 22	294	Massive gypsum layer	G + Q	17.9	b
	BA 21	285	Massive gypsum layer	G + Q	18.2	b
	BA 14	263	Laminated gypsum layer	G + A	18	b
	BA 13	250	Laminated gypsum layer	G + Q, A	18.3	b
	BA 11	237	Laminated gypsum layer	G + A, Q, C	16.8	b
Nahal Mishmar	MSH 43	566	Laminated gypsum layer	G + Q, A	19	b
	MSH 33	334	Laminated gypsum layer	G	19.4	b
	MSH 22	283	Massive gypsum layer	G	19.9	b
	MSH 11	208	Laminated gypsum layer	G	18.9	b
Nahal Mor	MR 40	545	Laminated gypsum layer	G + Q	19.1	b
	MR 20	470	Massive gypsum layer	G	18.5	b
	MR 10	410	Laminated gypsum layer	G	17.8	b
Mt. Izrach	HY1-Bulk	N/A	Bulk *aad*		−5.3	a
	HY-1	N/A	Aragonite laminae	A		
	HY2-Bulk	N/A	Bulk *aad*		−4.3	a
	HY-2	N/A	Aragonite laminae	A		
Deir Shaman	NT-B (NT 30)	N/A	Laminated gypsum layer	G + Q, A		
	NT-B (NT 20)	N/A	Massive gypsum layer	G		
	NT-B (NT 10)	N/A	Laminated gypsum layer	G + Q, A	28.3	a
	NT-B-110	N/A	Laminated gypsum layer		27.9	a
	NT-A-31	565	Laminated gypsum layer		17	a
	NT-A-22	505	Massive gypsum layer		17.3	a
	NT-B-21	N/A	Massive gypsum layer		18.8	a
	NT-A-21	503	Massive gypsum layer		19	a
	NT-A-11	464	Laminated gypsum layer		15.1	a
Perazim Valley	PZ1-B-2119	2119	Thick gypsum laminae (selenite)		19.4	c
	PZ1-B-2110	2110	Diss. gypsum in mixed layer		−18.8	c
	PZ1-B-2092	2092	Thick gypsum laminae (selenite)		17.7	c
	PZ1-B-1580 GYP 1	1580	Thin gypsum laminae (from detritus)		−13.7	c
	Pz7-30	423	Laminated gypsum layer	G + Q		
	Pz7-20	364	Massive gypsum layer	G		
	Pz7-10	326	Laminated gypsum layer	G		
	Pz1-31 (1)	451	Aragonite laminae	G + A, H	17.8	b
	Pz1-31 (3)	450	Laminated gypsum layer	G + H	18.8	b
	Pz1-30	390	Massive gypsum layer	G	19.2	b
	Pz1-29 (3)	330	Laminated gypsum layer	G	17.5	b
	Pz7-smr10	−280	Laminated gypsum layer (Samra Fm.)	G	16.1	a
Massada	Ms 202	2961	Laminated gypsum layer	G, B + Q	23.6	b
	Ms 201	2954	Laminated gypsum layer	G + Q	23.9	a
	Ms 205	2860	Aragonite laminae (CAS)	A + Q, C, D	21.1	c
	Ms 180	2807	Laminated gypsum layer	G + C, A	24.6	b,a
	Ms 172	2783	Laminated gypsum layer	G + Q	24.8	a
	Ms 171	2780	Massive gypsum layer	G + Q	25.6	a
	Ms 161	2753	Laminated gypsum layer	G + Q	25.7	b
	Ms 152	2705	Aragonite laminae (CAS)	A + Q	24.9	c
	Ms 151	2696	Laminated gypsum layer	G + H, Q, A	24.4	b
	Ms 140	2673	Massive gypsum layer	Anh + Q, A	28.3	b
	Ms 130	2654	Massive gypsum layer	G	27.7	b,a
	Ms-Top Gyp-Duplicate	N/A	Massive gypsum layer	Anh, B, G + Q, A	26.1	a
	Ms 125	2615	Bulk *aad*		−17.2	a
	Ms 900	2511	Gypsum concretion	G + Q, A, C	−12.1	a
	Ms 121	2505	Aragonite laminae (CAS)		26	a

(*continued on next page*)

Table 1 (*continued*)

Site	Sample	Elevation (cm)	Lithological type	Mineralogy	$\delta^{34}S$ (‰)	Lab
	Ms 121	2505	Aragonite laminae	A + C	−2.75	c
	Ms 110	2375	Aragonite laminae (CAS)	A + C, Q	19.8	a
	Nz 16-D	2286	Detritus laminae	C + Q, D, F	−7.8	a
	Ms 901	2241	Gypsum concretion	G + Q, A, C, H	−18.7	a
	Ms 100 Bulk	2058	Bulk *aad*	A + C, Q, H, D	−18.2	a
	Ms 100	2050	Aragonite laminae (CAS)	A + C	20.3	a,d
	Nz 15-D	1986	Detritus laminae	Q + C, D	−13.8	a
	Ms 902	1871	Gypsum concretion	H + G, A, C, Q	−19.8	a
	Ms 90	1813	Aragonite laminae (CAS)	A + C	13.6	c
	Ms 802	1721	Laminated gypsum layer	G + Q, C, H	22.6	a
	Ms 80	1640	Aragonite laminae (CAS)	A + C	20.2	c
	Ms 702	1489	Aragonite laminae (CAS)	A + C	−2.4	c
	Ms 74	1265	Massive gypsum	G + Q	21.9	a
	Ms 67a	1222	Detritus-halite laminae	H + A, Q, C	0.7	d
	Ms 75	1185	Aragonite laminae (CAS)	A + C, D	18.9	a
	Ms 67c	1055	Detritus-halite laminae	H + G, Q, A, C	9.7	d
	Ms 68b	1007	Bulk *aad*		−10.7	d,a
	Ms 61	832	Laminated gypsum layer	G + Q, A	20.4	b
	Ms 53	813	Laminated gypsum layer	G	20.5	b
	Ms 40	760	Laminated gypsum layer	G + Q, A	18.3	a
	Ms 38	730	Laminated gypsum layer	G + C, Q, A	19.0	a
	Ms 300-Bulk	707	Bulk *aad*	A, C, Q	−11.5	a
	Ms 300	705	Aragonite laminae (CAS)	A	19.8	c
	Ms 36	563	Laminated gypsum layer	G + Q, H, C	17.4	b
	Ms 35	554	Laminated gypsum layer	G + A, H	19.9	b
	Ms 34	553	Laminated gypsum layer	G + A, Q, H	19.1	b
	Ms 33	548	Laminated gypsum layer	G + Q, C	17.8	b
	Ms 37	546	Detritus laminae	Q, C, G	15.4	a
	Ms 32	544	Aragonite laminae (CAS)	A + C	17.8	c
	Ms 31.4	549	Native sulfur concretion gyp.crust	G + Q	15.6	b
	Ms 31.3	549	Native sulfur concretion gyp.crust	G + Q	13.2	b
	Ms 31.1	549	Native sulfur concretion	S + Q	−8.6	a
	Ms 28	504	Aragonite laminae	A + Q, C, H?	−14.4	a
	Ms 27	495	Native sulfur concretion	S	−11.7	a
	Ms 26	488	Aragonite laminae (CAS)	A + C	11.9	c
	Ms 25	483	Aragonite laminae	A + G	18.1	b
	Ms 24	481	Massive gypsum layer	G		
	Ms 23	480	Massive gypsum layer	G + A	19.1, 19	b,a
	Ms 221	477	Massive gypsum layer	G	18.8	a
	Ms 211	471	Gypsum laminae	G + H?, A, Q	17.4	a
	Ms 21	468	Gypsum laminae	G + A	18.9	a
	Ms-Gyp II-Duplicate	N/A	Massive gypsum layer	G	19.8	
	Ms 255	460	Gypsum laminae	G	15.6	d
	Ms 250	457	Aragonite laminae (CAS)	A + C	18.4	c
	Ms 145	430	Laminated gypsum layer	G + A, Q, C	18.2	a
	Ms 16	430	Aragonite laminae	A, G + C	17.8	b
	Ms 144	428	Laminated gypsum layer	G, A, Q, C	17.7	a
	Ms 15-1	426	Laminated gypsum layer	G	18.1, 17.6	a,b
	Ms 15-2	426	Laminated gypsum layer		18.1	b
	Ms 143	424	Laminated gypsum layer	G, A, Q, C + H?	18.7	a
	Ms 14-1	421	Laminated gypsum layer	G	17.8, 16.8	a,b
	Ms 14-2	421	Laminated gypsum layer		17.5, 18.1	b
	Ms 18	419	Laminated gypsum layer	G, + C, A, Q	16.3	a
	Ms 13-1	419	Laminated gypsum layer	G, A	17.6	b
	Ms 13-2	419	Laminated gypsum layer		17.7	b
	Ms 17	418	Red detritus laminae	B, G, Anh, A + H?		
	Ms 12	409	Aragonite laminae	A + Q, G, C		
	Mez 38 (1)	422	Laminated gypsum layer	Anh, G + Q, A		
	Mez 38 (2)	421	Laminated gypsum layer	Anh + G, A, H	18.5	b
	Mez 38 (3)	420	Detritus laminae	H + Anh, G, Q, C, D	11.7	b
	Ms 6	269	Bulk *aad*	A + Q, C, H	−16.5	a
	Ms 5	266	Aragonite laminae (CAS)	A	15.4	a
	Ms 1a	3	Bulk *aad*	H + Q, C, A	−12.5	a

Traces of minerals are preceded by "+".

Abbreviations: A, aragonite; G, gypsum; Q, quartz; H, halite; S, native sulfur; C, calcite; F, feldspar; D, dolomite; Anh, anhydrite; B, basanite; CAS, carbonate associated sulfate; N/A, not available. Elevation refers to height above the Samra–Lisan boundary. The labs in which the isotopic analyses were carried out are identified (see text for details): (a) University of Waterloo; (b) British Geological Survey; (c) University of Arizona; (d) Hebrew University of Jerusalem.

Table 2
Properties of primary gypsum layers in the Lisan Formation at the Massada site

Serial no.		Field name	Elevation above Massada section base (m)	Sedimentological classification	$\delta^{34}S$ (‰)	Measured gypsum layer thickness (cm)	Average gypsum content (%)	Gypsum content (g/cm^2)
8		Additional Gypsum	29.3–29.7	Laminar (gypsarenite)	23.5–24	40	85	68
7		Upper Gypsum unit (UGU)	25.85–28.13	~9 consecutive laminar and massive layers (gypsarenite and gypsite)	24.5–28	107	80	171.2
6		Broken gypsum	16.9–17.05	Laminar (gypsarenite)	22.5	16	70	22.4
5		Crenulated gypsum	12.36–12.55	Laminar (gypsarenite)	22	19	85	32.3
4	4.3	Small gypsum unit	8.13–8.24	Laminar (Detritus enriched, thin gypsarenite layer)	20.5	11	25	20.5
	4.2		7.87–8.07	Laminar (Detritus enriched, thin gypsarenite layer)	18.3	20	25	
	4.1		6.84–6.94	Laminar (Detritus enriched, thin gypsarenite layer)	19	10	25	
3		Lower Gypsum unit (LGU)	5.46–5.64	Laminar (gypsarenite)	17-20	18	88	31.7
2			4.68–4.82	Massive (gypsite)	17.5-20	14	70	19.6
1			4.18–4.29	Laminar (gypsarenite)	17.5-18.1	11	80	17.6

Total thickness of gypsum units 266 cm.
Total net-gypsum weight 383 g/cm^2.
Total net-sulfate weight 214 g/cm^2.
Average isotopic composition ~23.4‰.

The data is used to evaluate the total content of primary gypsum in the section as well as its average isotopic composition. Calculations assume a gypsum density of 2 g/cm^3. The gypsum content in layers 2 and 3 was determined by sampling sediment cores and analyzing them for water-soluble sulfate. The result was used to determine the gypsum content in the other layers. The net gypsum thickness of the UGU is calculated as 80% of 107 cm, i.e., ~85 cm.

Table 3
Summary of the sulfur content (expressed as sulfates) and isotopic compositions of the different sulfur occurrences at M1 site near Massada

	Primary gypsum layers	Low $\delta^{34}S$ sulfur	Carbonate associated sulfate	Total
Sulfate content (g/cm^2)	214 (±40)	135 (±90)	10	359 (±130)
Average isotopic composition (‰)	23.4	−15	~17	**10.7 (5.8–15.5)**

Values in parentheses represent uncertainties stemming from thickness measurements (±10%) and gypsum content estimates (±10%).

The irregularly shaped concretions are 0.1–2 cm in diameter. Frequently the core of larger concretions consists of native sulfur. The disseminated gypsum is present in aragonite laminae, and was identified by SEM and by the chemical analyses of water-leachates of aragonite. The isotopic composition of this group is significantly ^{34}S-depleted ($\delta^{34}S = -26$ to 1‰).

3.1.3. Native sulfur

S° typically appears as rounded concentrations, 1–10 cm in diameter, occasionally nested in red gypsum crusts, and offsetting surrounding layers. Isotopic compositions are in the range of $\delta^{34}S = -20$ to −10‰.

3.1.4. Carbonate associated sulfate

Acid-dissolved aliquots of thoroughly water-leached aragonite indicate that sulfate co-precipitated with this mineral. Sulfate average concentration is 4800 (±1500) ppm and its isotopic composition is in the range of $\delta^{34}S = -2.5$ to 26‰.

3.2. Bulk isotopic composition of sulfur

A detailed account of the distribution and isotopic composition of sulfur in the primary gypsum layers at the Massada M1 site is given in Table 2. The total amount of sulfate associated with this group is 214 g/cm^2.

The low $\delta^{34}S$ gypsum described in Section 3.1.2 comprises 1–5 wt% of the 2700 cm thick aragonite–silty detritus bundles (see Appendix A), equivalent to 90 $g_{(sulfate)}/cm^2$, on average. We estimate the native S° content to be about half the amount of sulfur comprising the isotopically-light gypsum (Section 3.1.2), bringing the combined sulfate content of both groups to 135 g/cm^2 in the Massada M1 section. The mass of aragonite-associated-sulfate (total thickness of 1400 cm, bulk density of 1.5 g/cm^3, $[SO_4^{2-}] = 4800$ ppm) amounts to ~10 g/cm^2.

The total sulfate content in the various occurrences listed above amounts to ~360 g/cm^2, yielding a bulk sulfur isotopic composition in the Lisan Fm. of $\delta^{34}S = 10.7$‰ (Table 3). This value is within the range of the estimated bulk isotopic composition of sulfur input into the lake of $\delta^{34}S \approx 6$–14‰ (Torfstein et al., 2005).

3.3. $\delta^{34}S$ values in the Holocene En-Gedi core

The isotopic composition of sulfur in the Holocene Ze'elim Fm. was determined for samples collected from the 20 m long En-Gedi core (Table 4; Migowski et al., 2004, 2006). Of the eight samples analyzed, four are gypsum laminae, and four are disseminated gypsum extracted by H_2O-leaching from dark-brown marls. The isotopic composition of sulfur in the En-Gedi core is 15‰ ± 0.7 (1σ; Table 4).

4. DISCUSSION

4.1. Limits on sulfate concentration in the lakes

In the Ca-chloride Lake Lisan brine, high Ca^{2+} concentration would not be significantly modified by mineral precipitation or dissolution; rather, it would display a relatively conservative behavior whereby Ca^{2+} concentration reflects the degree of dilution of the brine. In contrast, dissolved sulfate concentration in the lake would be dictated by the rate of sulfate inflow, gypsum solubility and Ca^{2+} concentrations. Thus, the lower the salinity and Ca^{2+} concentration, the higher the SO_4^{2-} concentration before gypsum saturation is reached.

Katz et al. (1981) and Krumgalz and Millero (1983) determined that maximum gypsum solubility (in a Dead Sea-like brine) is reached when modern Dead Sea brine is diluted by about 3-fold. Further dilution is accompanied by a decrease in gypsum solubility. Hence, a 3-fold diluted Dead Sea brine implies calcium concentrations of approximately ~5500 mg/l (a third of the 16.7 g/l concentration of the upper water body in the 1960's Dead Sea; Neev and Emery, 1967). Gypsum saturation in such a brine would be reached at ~3000 mg (SO_4^{2-})/l (as calculated following Krumgalz and Millero (1983) as well as by the PHREEQC code (Parkhurst and Appelo, 1999)). Katz et al. (1981) conducted mixing and evaporating experiments of seawater and Dead Sea water. Extrapolation of their data agrees well with the above calculations and suggests that brines displaying sulfate concentrations of 3000 mg/l would be only slightly oversaturated with respect to gypsum.

During its last and highest high stand (~27 to 17 ka BP; Fig. 2), Lake Lisan's volume was ~3-fold larger than that of the mid 20th century Dead Sea and thus, a corresponding bulk dilution of the Lisan water column was assumed (Neev and Emery, 1967; Begin et al., 2004). Water column stratification however, would mean that the dilution of the monimolimnion was lower and that of the mixolimnion higher than described above. Nevertheless, for the following calculations and discussion, we assume that the upper most limit on sulfate concentrations in Lake Lisan was 3000 mg/l. Lower values would further support our model.

4.2. Sulfur mass balances

In the following section we present two independently calculated mass balances related to the sulfur system in Lake Lisan, which are not consistent. Resolving the source of the difference between the two calculations provides insight into the limnological and hydrological evolution of Lake Lisan. We focus the calculation on the Upper Gypsum Unit (UGU), where a striking quantitative difference

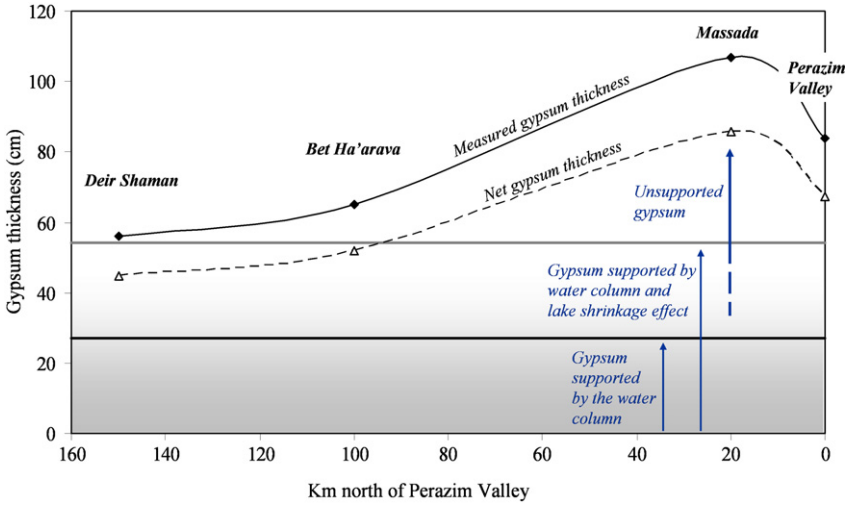

Fig. 5. Measured thicknesses of gypsum in the UGU in 4 sampling sites along the Dead Sea rift compared to maximum water-column-supported gypsum thicknesses. Both the measured and net (pure gypsum comprising some 80% of the measured thickness) thicknesses are presented. Under the constraints detailed in the text and assuming water level decline of 100 m, the lake water column sulfate reservoir could support the deposition of up to 27 cm of primary gypsum. This value is doubled when allowing for lake shrinkage during level drop, and the consequent accumulation of gypsum on the remaining lake floor. Even under these maximal calculations, only ~60% of the net thickness of the UGU in the Massada section (~85 cm) can be accounted for. In the northern Deir Shaman and Bet Ha'arava sites, where there seems to be an agreement with UGU thicknesses, the lake shrinkage would have less of an impact on gypsum thickness because of their relatively marginal location.

Table 4
$\delta^{34}S$ values in the Holocene En-Gedi core

Sample name	Lithology	Depth (m)	Age (a BP)	$\delta^{34}S$ (‰)
DSEn B2	Gypsum laminae	2.15	2058	14.3
DSEn B2	Diss. gypsum	2.17	2068	14.2
DSEn A5o	Diss. gypsum	4.18	3025	16.2
DSEn A8o	Diss. gypsum	9.12	5378	14.7
DSEn A8o	Gypsum	9.64	5625	14.7
DSEn A10u	Diss. gypsum	13.12	7282	15
DSEn A10u	Gypsum laminae	13.7	7558	15.1
DSEn A103u	Gypsum laminae	17.51	9373	15.6

The samples are either sedimentary gypsum laminae or disseminated gypsum. All exhibit a homogeneous value of 15 ± 0.7‰ (1σ). Ages are derived from calculated regression ages based on the data of Migowski et al. (2004).

between the sulfate input and precipitating gypsum is evident. Similar discrepancies, though of smaller magnitude, are evident in the other primary gypsum layers as well. The properties of the UGU (spatial distribution, thickness and age), which are well-known, provide strong constraints on the lake setting during its precipitation and can be used to reconstruct the limnological history during other gypsum-precipitation stages.

The UGU precipitated after a significant lake level drop of ~100 m, which in turn, came after a long high-stand period (27–17 ka BP; Fig. 2). U–Th dating of primary aragonite (below and above the UGU) indicates that the unit, was deposited over a ~1 to 2 ka period (~17–15 ka BP; Haase-Schramm et al., 2004). It is the thickest primary gypsum unit deposited in the DSR during the past 70 ka (~230 cm at the M1 Massada site). Yet, the UGU is not homogeneous and contains sequences of alternating aragonite-detritus (*aad*) (Fig. 2; Table 2) that indicate changes in the depositional conditions in the lake. The net gypsum thickness at the M1 site is estimated as 85 cm.

Fig. 6 presents the calculated thickness of gypsum as a function of lake level drop and sulfate concentration in the water column at the onset of water level decline. Under optimal conditions, i.e. a 100 m lake level decline and maximum sulfate concentration (3000 mg/l), no more than ~ 27 cm of gypsum could have precipitated from the water column. This corresponds to only 30% of the net gypsum thickness of the UGU in the Massada M1 site, implying that a significant fraction of the sulfate comprising the UGU could not have been derived directly from the water column during lake level drop; thus, an additional source of sulfate is required for the precipitation of the UGU. This "excess sulfate" must have been derived from outside the main lacustrine water body.

Allowing for 50% decrease in lake surface area due to lake level decline (Hall, 1997; Bartov et al., 2002, 2003)

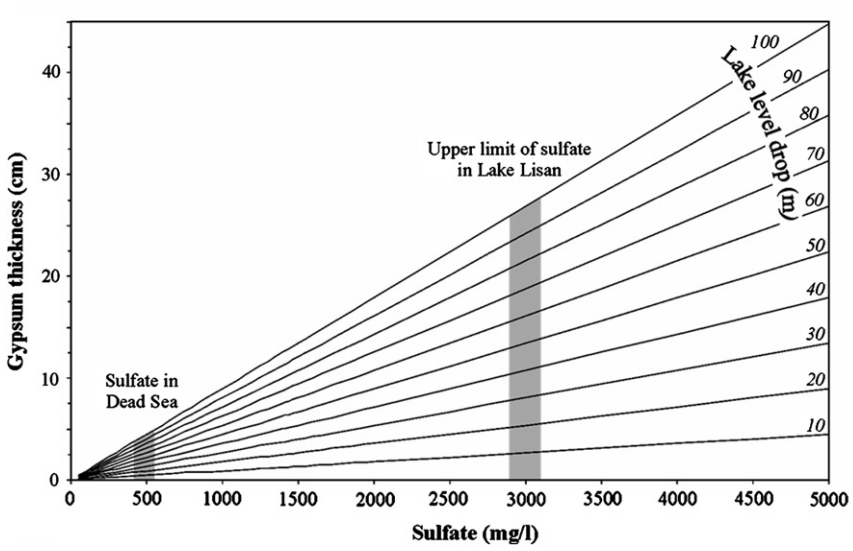

Fig. 6. Calculated thickness of gypsum as a function of lake level drop and sulfate concentration in the water column at the onset of water level decline. Even under optimal conditions (100 m lake level drop, $[SO_4^{2-}] = 3000$ mg/l) the maximum thickness of primary gypsum deposits would have been less than 30 cm, i.e., only ~30% of the observed UGU thickness in Massada.

supports the deposition of a 2-fold thicker gypsum layer, bringing the upper limit of its thickness to ~54 cm or 60%. The remaining ~40% "excess sulfate" is not accounted for. The thickness of the UGU decreases gradually from the lake center (Massada site) towards its northern and southern margins (Fig. 5). When considering the effect of the shrinkage of the lake, the UGU thickness in the northern Deir Shaman and Bet Ha'arava sites (Fig. 1) could have been supported by the water column sulfate reservoir. On the other hand, the lake shrinkage is expected to have less of an impact on gypsum thickness in these relatively marginal sites, which were submerged under a thinner water column for a shorter time, compared to more central sites.

Mass balance calculations and isotopic compositions constrain the origin of the excess sulfate. The bulk $\delta^{34}S \approx 10.7‰$ in the Lisan Fm. (Table 3) is consistent with the suggestion that the main source of sulfur in Lake Lisan was incoming freshwater (e.g., paleo-Jordan River), which display a similar $\delta^{34}S$ value (Torfstein et al., 2005).

Given that the lake received a freshwater load of 2–3 m/y containing 20–120 mg/l of dissolved sulfate (Torfstein et al., 2005) the total amount of sulfate supplied to the lake via freshwater during its ~50 ka life span was calculated to be within ~200 to 1800 g/cm^2. The lower value of this range is in agreement with the total amount of sulfate in the Massada section (~360 g/cm^2; Table 3).

An estimate of the sulfur mass balance for shorter periods is also consistent with observations; over the ~10 ka high-stand period that preceded the deposition of the UGU, the total amount of sulfate that entered the lake was 50–360 g/cm^2, equivalent to 90–645 $g_{(gypsum)}$/cm^2, in agreement with the gypsum content of the UGU (~170 $g_{(gypsum)}$/cm^2). Thus, the quantitative and qualitative consistency between the sources and sinks of sulfur in Lake Lisan over long and short periods indicate that the bulk of sulfur that entered the lake was from freshwater sources.

Fig. 7. Schematic representation of the limnological–hydrological settings of groundwater flow during high and low stands and intermediate transient stages. The extent of the lake expansion and the displayed $\delta^{34}S$ values relate to the most extreme event of gypsum deposition in Lake Lisan, the Upper Gypsum Unit. (1) During prolonged low stands (high salinities) the lake is relatively depleted in sulfate (10–15 ‰) and attains $\delta^{34}S$ values close to those of the water sources. This situation is analogous to the present day Dead Sea. (2) As the climate shifts towards wetter conditions, the limnological–hydrological system responds by a lake level rise accompanied by fluid infiltration into adjacent strata. During this period the fresh groundwater table migrates upwards because of the increased elevation of the drainage base. Note the differences between adjacent strata lithology on both sides of the basin. To the West of the Dead Sea, subsurface strata are comprised mainly of limestone and dolomite (Upper Cretaceous Judea Group), while to the East, most of the exposed section and the subsurface is composed of permeable sand units (Cambrian), dolomite and limestone (Jurassic, Cretaceous). The crystalline basement rocks (Precambrian granite) have low permeability and groundwater seepage through them is limited (Stanislavsky and Gvirtzman, 1999). (3) When steady state high stand conditions are achieved, lake-derived solutions continue to percolate into the subsurface. At the same time, the development of anoxia in the monimolimnion results in sulfate ^{34}S-enrichment (up to ~40‰; Torfstein et al., 2005). In the mixolimnion, sulfate isotopic values (~10‰) approach those of freshwater sources. (4) Following climate change and lake level decline, the flow direction of the saline groundwater is reversed. Prolonged gypsum precipitation, which began as a result of water column overturn and mixing (but quickly exhausts the lake sulfate reservoir) is enabled through the ongoing out-flushing of groundwater back into the lake. The higher and wider the lake was during the preceding high stand, the more sulfate-laden groundwater is flushed back to the lake. The sulfur isotopic composition of the returning fluids reflects the bulk isotopic composition of the water column during the preceding high stand.

The problem, however, is that accumulating this amount of sulfate in the water column *prior* to massive gypsum precipitation is not possible due to the upper limits on sulfate concentration in the brine.

The ~40% "excess sulfate" is a *minimum* figure because the calculations refer to optimal conditions (highest possible sulfate concentrations in the precipitating solution, net thickness of gypsum in sediments and a full effect of sediment thickening due to decrease in lake size). In practice, the amount of "excess sulfate" that was reflushed to the lake during its water level decline was probably larger.

4.3. The source of the "excess sulfate" and temporal migration of lake solution into adjacent strata

The short duration of the deposition period of the UGU (<2 ka) did not provide ample opportunity for the "typical" freshwater sulfate ($\delta^{34}S \approx 10‰$; $[SO_4^{2-}] < 120$ mg/l) to accumulate. Lake level drops were

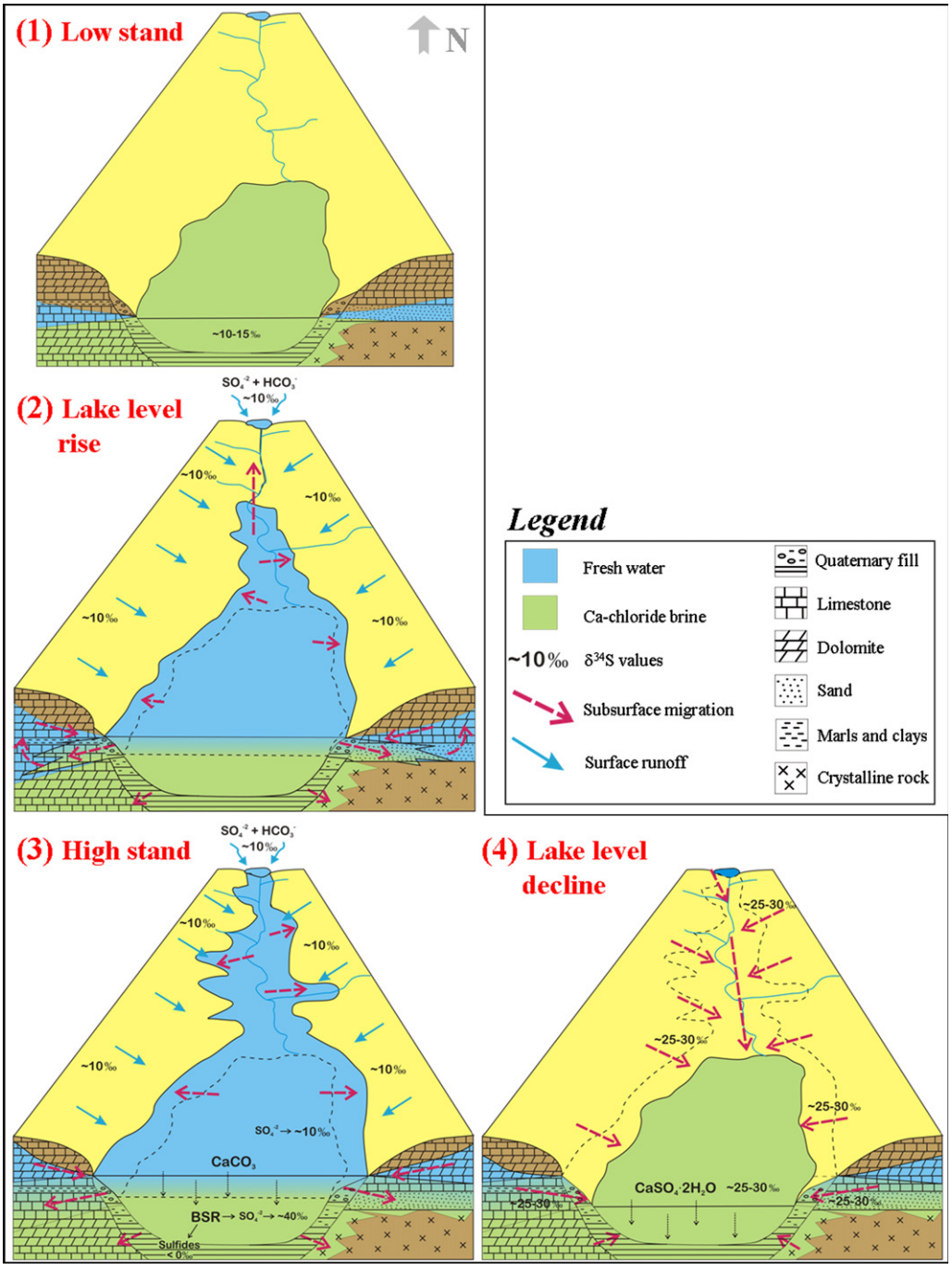

induced by a decrease in the water inflow and hence, the freshwater sulfate input to the lake was low at this stage. In addition, the lake level drop resulted in overturn which lead to the oxidization of the water column, thereby inhibiting further BSR and ^{34}S-enrichment of dissolved sulfate anions. Thus, the excess sulfate introduced into the lake once gypsum precipitation began at ~17 ka BP, *must* have already been predominantly ^{34}S-enriched ($\delta^{34}S \approx 25$–$28‰$). The possibility that part of the UGU was derived by dissolution of old (Neogene) gypsum units in the Jordan River basin is ruled out since they are characterized by significantly lower δ^{34}S values (16–23‰; Raab et al., 1997, 2000). Given the spatial and temporal uniform isotopic composition of the UGU (Figs. 3 and 4) it is concluded that both sulfate reservoirs (sulfate dissolved in the water column and sulfate from the external sources, i.e., the "excess sulfate") had a similar ^{34}S-enriched isotopic composition, which record similar geochemical evolutionary paths.

We propose that the source of the excess sulfate is high-δ^{34}S saline groundwater flowing from the lake margins and adjacent strata into the lake following its decline. These solutions penetrated the subsurface during the preceding high-stand period, when the lake covered large areas of the DSR. Upon the transition to dryer climatic conditions and lake level decline, the solutions were flushed back to the receding lake, replenishing its sulfate reservoir and enabling further gypsum precipitation (Fig. 7).

Evidence for hypersaline groundwater with high δ^{34}S values (30–60‰) is provided by gypsum-saturated solutions recovered by Gavrieli et al. (2001) from shallow boreholes drilled along the shores of the Dead Sea. These were suggested to represent residual interstitial water in the sediments, where BSR processes lead to ^{34}S-enrichment of residual dissolved sulfate. ^{34}S-depleted sulfur phases observed within aragonite–silty detritus (*aad*) sequences in the Lisan sediments (Fig. 4; Table 1) suggest that similar brines with high δ^{34}S values formed during the Lisan period, too. These however, are absent in the *aad* sequences (see Torfstein et al., 2005).

These brines should not be confused with the deep subsurface brines that currently discharge into the Dead Sea as thermal springs (e.g., the Qedem springs) and might have also been discharging during Lake Lisan period. These display half the salinity of the Dead Sea, are undersaturated with respect to gypsum and are characterized by $\delta^{34}S_{(SO_4)} \approx 22‰$ (Gavrieli et al., 2001), i.e., lower than needed to replenish the water column during the UGU precipitation.

4.4. Hydrologic controls and processes in the Dead Sea Basin

The formation and discharge of the two above-mentioned types of brines, i.e., the deep-thermal springs and shallow ^{34}S-enriched brines, are controlled by two different hydrological processes. The first, is controlled by the past intrusion of the Pliocene Sedom Lagoon water into its surroundings and the formation of the Ca-chloride Dead Sea type brine (Starinsky, 1974). Density-driven flow associated with salinity variations was the principal driving force that caused large-scale migration of brine into the surrounding aquifers. The hypersaline-heavy brines sank into the sediment fill of the DSR and migrated laterally into deep aquifers during the past 3–6 Ma (Stanislavsky and Gvirtzman, 1999; Gvirtzman, 2006). The present discharge of these deep brines to the surface, in the form of thermal-salty springs (e.g., Qedem spring), is probably controlled by the hydraulic head generated in the surrounding mountains (Goldschmidt et al., 1967; Stanislavsky and Gvirtzman, 1999; Gvirtzman, 2006). A decrease in the hydraulic head during dry periods (which were characterized by low lake stands) and subsequent weaker leaching of the brines via the circulation of meteoric water would lead to a *decrease* in their discharge. Thus, these brines and this process could not provide the missing sulfate to the lake.

A second important hydrological process in the DSR is the adjacent groundwater system connected hydraulically to the Dead Sea (and formerly to Lake Lisan) which serves as a terminal drainage base for groundwater flow (Yechieli, 2006; Gvirtzman, 2006). Changes in the drainage base level for the groundwater flow, i.e., the lake level of Lake Lisan and the Dead Sea, could have a significant effect on the groundwater flow regime. Given the amplitude of lake level fluctuations during the last 70 ka ($\Delta \approx 190$ m during the Lisan time, and more than 200 m upon the transition from Lake Lisan to the Holocene Dead Sea; Fig. 2), the volume and extent of the above active aquifers were probably larger during high stand stages.

During prolonged periods of Lake Lisan high stands, large areas in the DSR were submerged and adjacent strata became saturated with brine. Following temporal lake level drops some of these areas were exposed and the brines contained within them were flushed out (Fig. 7). The fraction of excess sulfate in primary gypsum beds is therefore correlated with the degree of lake level decline and sediment exposure; The larger the lake level drop, the more sediment exposed and the thicker the gypsum bed that precipitated thereafter. Significant deposition of gypsum was invoked not only by increasing salinity of the water column but also because of increased inflow of sulfate-rich brines flushed from the surrounding aquifers. Accordingly, the thickness of a specific gypsum bed is expected to rise towards lake center due to the growing contribution of excess sulfate to sites which are submerged longer and under a thicker column of water (similar evaporitic thickness gradients are reported in deep water settings elsewhere; e.g., the Mediterranean Messinian (cf. Rouchy and Caruso, 2006)). This is best exemplified by the properties of the UGU, deposited during the final decline of Lake Lisan. Fig. 5 shows that in all studied sections the UGU's thickness either reaches the uppermost calculated limit (e.g., the northern Deir Shaman site) or significantly exceeds it (e.g., the central Massada site).

During stages of limited lake level fluctuations and subsequent minimal sediment exposure (which are typical of the Holocene low-stand water body) only little or no

primary gypsum precipitation was invoked. Such limnological conditions also prevented significant BSR-related isotopic fractionation. Thus, the small amount of primary gypsum that did precipitate does not display $\delta^{34}S$ values much higher than the upper boundary of the inflowing sulfate ($\delta^{34}S \approx 6$–$14‰$).

4.5. Hydrological–limnological implications

Below, a rough estimate of the volume and locus of the subsurface sulfate-bearing solutions is calculated assuming sulfate concentrations of 3000 mg/l and average rock porosity in the DSR region of 10% (Gvirtzman et al., 1997; Gvirtzman and Stanislavsky, 2000; Gvirtzman, 2006). Assuming that 40% of the ~85 cm-thick UGU at Massada could not have been supported by direct precipitation from the water column (see calculations in Section 4.2) and that the "excess sulfate" (equivalent to ~38 g $(SO_4^{2-})/cm^2$) is spread over an area ranging between 750 and 1600 km^2 (corresponding to elevations of 400 mbsl (the approximate elevation of the 20th century Dead Sea) and 330 mbsl (the elevation of Massada UGU), respectively), the corresponding volume of groundwater that was flushed to the lake was between 950 and 2024 km^3, respectively. For a 220 km long lake (ca. length of the high-stand of Lake Lisan; Begin et al., 1974) and a ~200 m thick groundwater table (roughly corresponding to the amplitude of lake level changes during the last 70 ka), these volumes correspond to lateral brine migration in the range of ~11 to 23 km east and west of the lake. This range is of course highly sensitive to the uncertainties in the amount of "excess sulfate", in the changes in lake's dimensions and the host-rock properties. Furthermore, the percolating solutes probably did not spread symmetrically east and west and along a single front line but rather, flowed along layers with preferable permeability and high porosity. They could have penetrated the western escarpment, composed mainly of Cretaceous carbonates, the eastern escarpment, composed of Cambrian sandstones together with Jurassic and Cretaceous carbonates (Fig. 7) and/or could have expanded southward into the Neogene (Hazeva Fm.) and Quaternary (Dead Sea Group) sedimentary fill (Fig. 1). The abundant fault lines along the DSR probably allowed vertical flow, further hindering more precise estimate of the flow path of the percolating brine.

The main constraint on the volume and locus of the sulfate-bearing solutions is the possible flow rate in the subsurface: the conceptual model requires groundwater to migrate at least several km in and out of the surrounding aquifers over a time period of several ka. Previous studies and modeling of groundwater in the DSR indicate that such rates are possible and reasonable (Hurwitz et al., 2000; Yechieli, 2000, 2006; Laronne Ben-Itzhak and Gvirtzman, 2005). For example, the rapidly receding level of the Dead Sea over the last decades led to the exposure of wide coastal areas which were covered by the Dead Sea water only 10-30 years ago are currently flushed out and dry (Yechieli, 2006).

The evolution of the high $\delta^{34}S$ isotopic composition of the "excess sulfate" could have been achieved through BSR in the subsurface or in the lake's water column. Once subsurface penetration took place, sulfate ^{34}S-enrichment in the groundwater was limited by the availability of organic matter. Consumption of sulfate by BSR would result in the lowering of sulfate concentrations (Eq. (1)) which would mean that the calculated volume of groundwater would be significantly larger, which does not seem reasonable. Though subsurface gypsum dissolution could compensate for such a decrease in sulfate concentrations, the correspondence between quantities and isotopic compositions of sources and sinks indicates that significant dissolution of gypsum in the subsurface is unlikely. On the other hand, the spatial and temporal homogeneity of the Upper Gypsum Unit (Fig. 4) indicate that $\delta^{34}S$ values in the proposed groundwater sulfate reservoir must have been similar to that of the mixed water column. The high-$\delta^{34}S$ value of the replenishing brine probably reflects BSR that took place in the lake monimolimnion before the brine infiltrated into the subsurface. Thus, the infiltrating fluids represent a mixture of mixolimnion and monimolimnion. Such mixture could however occur both before migration into the subsurface (along the redoxcline) but also, and perhaps mainly, during the subsurface cycling of these solutions (Fig. 7).

4.6. The deposition of the lower gypsum unit

The limnological history of Lake Lisan during MIS4 (70–56 ka BP) is less established than that of the MIS2 period (e.g., lake levels in Fig. 2). The stratigraphic section of the Lisan Fm. shows a sequence of laminated primary aragonite (the *aad* facies) that was deposited after the desiccation of Lake Samra (~70 ka BP), marking a resumption of high stand conditions due to new freshwater input. In the PZ1 site (Fig. 1), the four meters of *aad* between the base of the section and the Lower Gypsum Unit (LGU; Fig. 2) were dated by U–Th, showing that deposition was interrupted sometime between 67 and 60 ka BP (Haase-Schramm et al., 2004). The LGU, which was deposited between 58 and 56 ka BP (Haase-Schramm et al., 2004), consists of three primary gypsum layers whose individual thicknesses in the M1 site are 10 cm (laminated layer), 10 cm (massive layer) and 16 cm (laminated layer) (Fig. 2). Similar to the UGU, the thickness of these layers decreases laterally and their isotopic compositions are spatially and temporally uniform ($\delta^{34}S$ between 17 and $20‰$). According to this stratigraphic record, lake level during MIS4 receded at least once from the PZ1 sampling site. Short-term fluctuations in the lake level and overturn of the water body would not allow a prolonged build-up of the ^{34}S-enriched sulfate reservoir and are thus consistent with the relatively low $\delta^{34}S$ values and the relatively thin gypsum layers in the LGU compared to the UGU.

The cyclic deposition of primary gypsum layers over short time periods (the UGU and LGU are comprised of 9 and 3 individual gypsum layers, respectively) implies that the flow-back of sulfate-bearing groundwater to the lake

and subsequent gypsum precipitation took place during very short events (several tens of years), which were intermitted by short resumptions of *aad* precipitation in the lake.

4.7. The transition from Lake Lisan to the Holocene Dead Sea

The sediments comprising the Quaternary lacustrine deposits in the DSR are characterized by sharp lithological changes that coincide with global climatic shifts. The best example of such are the contacts between the Lisan Fm. and the sediments that under- and over-lay it. Whereas the last glacial Lisan Fm. contains a high fraction of primary minerals (aragonite and gypsum; >60%) the under- and over-laying sequences (Samra and Ze'elim Fms., coinciding with the last and present interglacials, respectively) contain a much lower percentage (<20%) of primary minerals. In general it may be stated that the DSR lakes oscillated between periods of low stand allochtonous deposition to high stand aragonite–gypsum deposition periods. The deposition of large amounts of primary gypsum requires an active hydrological system which supplies large amounts of dissolved sulfate to the lake over short time frames, enables their subsurface cycling in adjacent strata, and finally, enables massive sulfate discharge back into the lake over short periods. These processes are associated with an overall wet stage although the deposition of primary gypsum takes place during short-term shifts towards dryer conditions (Stein et al., 1997; Bartov et al., 2003; Haase-Schramm et al., 2004).

The Holocene sedimentary sequence is characterized by scarcity of gypsum (Migowski et al., 2004, 2006). The gypsum that is present in the section appears in the form of thin laminae or disseminated gypsum with a relatively uniform $\delta^{34}S$ value (15 ± 0.7‰; Table 3), which is similar to that of the modern Dead Sea solution (14.5‰; Gavrieli et al., 2001). This is the result of a limited sulfate supply to the Holocene Dead Sea and diminished BSR processes compared to the Lisan time. Nevertheless, the BSR that did take place resulted in a shift of the $\delta^{34}S$ values of the Holocene Dead Sea to values slightly above the upper boundary of the estimated freshwater inflow to the lake (i.e., 6–14‰).

This also suggests that flushing of Lisan-time sulfate from adjacent strata must have been completed before the final transition to the Holocene Dead Sea (~14–10 ka BP; Stein, 2001) and that sulfate contained in the Holocene Ze'elim Fm. was introduced to the lake after the above transition and is not Lisan remnant sulfate.

The last interglacial Samra Fm. (see Waldmann et al., 2007) also contains a lower fraction of primary minerals compared to the Lisan Formation. Thus, it seems that the limnological–hydrological conditions during this time were similar to those that existed throughout the Holocene, i.e., a relatively dry period during which lake levels were relatively low. This is supported by a low $\delta^{34}S$ value (16.1‰) measured in primary gypsum located approximately 3 m beneath the Samra–Lisan transition in the Perazim Valley.

Because the distribution and isotopic compositions of primary gypsum in the DSR lacustrine deposits reflect the regional climatic–hydrologic conditions (Fig. 8) the possibility arises to use these for qualitative reconstruction of the limnological-climatic history of older lacustrine deposits in the Dead Sea Basin (e.g., the Samra Fm. and Mid-Pleistocene Amora Fm.; Torfstein et al., 2007). These insights could also be applied for the study of other sedimentary sections with similar characteristics.

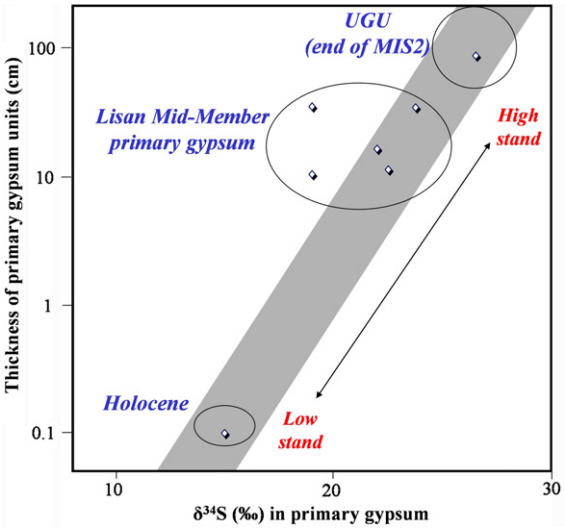

Fig. 8. Schematic presentation of the connection between the thickness of primary gypsum layers, their $\delta^{34}S$ values and their relation to climate. Three arrays are observed: Holocene, Lisan Mid-Member gypsums, and Lisan UGU. These represent the two extremes of dry (Holocene) and wet (MIS-2 which ended with the deposition of the UGU) climates, as well as intermediate stages.

5. CONCLUSIONS

(1) Sulfur occurs in the late Pleistocene Lisan and Holocene Ze'elim Formations in a variety of forms, each characterized by specific sedimentologic properties and isotopic compositions. The main sulfur reservoir in the sediments, primary gypsum, is ^{34}S-enriched (14–28‰) compared to the other sulfur reservoirs and compared to the source of sulfur to the lake (~10‰). The isotopic shifts are attributed to bacterially-mediated sulfate reduction and concurrent isotopic fractionation, that took place in the lower anoxic water body (monimolimnion) during high stand stages.

(2) Following climatic shifts and lake level decline, the water column overturned, mixed, oxidized and precipitated primary gypsum. Nevertheless, given the maximum sulfate solubility in the lake water, the water column sulfate reservoir could have only supported the deposition of up to 60% of the mass of the exposed gypsum layers.

(3) The relationship between the bulk isotopic composition and quantities of sulfur in the sources and sinks of the Lisan lacustrine system, indicates that the excess (i.e., mass balance-unsupported) sulfate in primary gypsum layers was derived from dissolved sulfate in solutions that were discharged into the lake from the surrounding marginal sediments and wall-rocks of the basin during episodes of lake level decline. The source of this recharged sulfate were lake solutions that penetrated the subsurface during the preceding high-stand stage. The lateral penetration of these subsurface brines was significant and could have reached a distance of up to ~20 km from the lake.

(4) During its high-stand, Lake Lisan was relatively enriched in dissolved sulfate, precipitated aragonite, and accommodated extensive BSR activity as well as extensive percolation of sulfate-bearing solutions into the basin bedrock and margins. Following lake level drop, ^{34}S-enriched subsurface solutions were flushed back to the shrinking lake and provided the water column with sulfate, thereby enabling the continued precipitation of significant quantities of ^{34}S-enriched primary gypsum. In contrast, diminished supply of freshwater sulfate and bicarbonate to the low level Holocene Dead Sea resulted in little or no primary gypsum deposition and only small amounts of aragonite in the sediments. In addition, $\delta^{34}S$ values in Holocene sediments show no evidence for mixing with higher $\delta^{34}S$ "Lisan" sulfate. Hence, the sulfate observed in the Holocene sediments was introduced to the lake environment after the desiccation of Lake Lisan.

(5) The thicknesses and $\delta^{34}S$ values of primary gypsum layers in the sedimentary column reflect the difference between the overall wet high-stand and dry low-stand stages in the evolution of the Upper-Quaternary Dead Sea basin lakes. These can be used to reconstruct the hydrological–limnological evolution of Lake Lisan (i.e., the deposition of the UGU took place after the long high stand of MIS 2 compared to the deposition of the LGU which occurred after the shorter high stand of MIS4).

(6) Similar inferences can be applied to the earlier history of water bodies in the Dead Sea basin (e.g., Lakes Amora and Samra) as well as to other deep water gypsum-precipitating water bodies. Given the general tendency to overlook the lake-groundwater interaction in evaporite-precipitating environments, the reported gypsum-related mass balance considerations and the proposed model for resolving the excess sulfate problem, should be considered in future studies of lacustrine and marine evaporitic sequences.

ACKNOWLEDGMENTS

We thank A. Amrani and Z. Aizenshtat for advice and support in laboratory work and E. Shalev for valuable discussions. We also thank Blair Jones and two anonymous reviewers for helpful and constructive remarks. The study was supported by BSF 2000271 (to I.G. and M.S.) and GIF 717.129.8/2001 (to M.S. and Y.K.).

APPENDIX A

Gypsum concentration (% wt.) in different lithological types in the Massada M1 section, as determined from H_2O-leaching experiments. Aaragonite laminae yielded practically no gypsum, while all (except one) bulk *aad* samples contain a significantly larger amount of gypsum (1.1–4.8%)

Sample	Lithology	Elevation (cm)	Gypsum (% wt.)
Ms 205-B	Bulk *aad*	2870	0.1
Ms 125-c	Bulk *aad*	2615	3.3
Ms 121	H_2O leached aragonite	2504.5	0.2
Nz 16-D	Detritus laminae	2285.5	0.5
Ms 100-Bulk	Bulk *aad*	2058	2.1
Ms 100	H_2O leached aragonite	2050	0.0
Nz 15-D	Detritus laminae	1985.5	1.1
Ms 67-A	Mainly halite	1221.8	3.5
Ms 75-D	Detritus laminae	1187.8	0.8
Ms 67-B	Mainly halite	1115	1.1
Ms 67-C	Mainly halite + gypsum	1055	25.9
Ms 68-b	Bulk *aad*	1006.5	1.1
Ms 67-D	Mainly halite	991.5	0.2
Ms 67-D	Mainly halite	991.5	0.5
Ms 300-B	Bulk *aad*	672	4.7
Ms 28	Bulk *aad*	504	4.2
Ms 6	Bulk *aad*	269.3	4.8
Ms 1-a	Bulk *aad*	3	2.4

The bulk *aad* samples, considered to best represent the gypsum content in the *aad* sections, have more gypsum than both the aragonite and detritus laminae. This is probably due to selective laminae separation procedures which discriminated against the incorporation of small gypsum crystals, present in the vicinity of the treated laminae into the above fractions, while bulk *aad* samples were coarsely extracted from the field samples with no such discrimination.

REFERENCES

Anderson R. Y., Dean W. E. J., Kirkland D. W. and Snider H. I. (1972) Permian Castile varved evaporite sequence, West Texas and New Mexico. *Geol. Soc. Am. Bull.* **83**, 59–85.

Bartov Y., Goldstein S. L., Stein M. and Enzel Y. (2003) Catastrophic arid episodes in the Eastern Mediterranean linked with the North Atlantic Heinrich events. *Geology* **31**, 439–442.

Bartov Y., Stein M., Enzel Y., Agnon A. and Reches Z. (2002) Lake levels and sequence stratigraphy of Lake Lisan, the late Pleistocene precursor of the Dead Sea. *Quat. Res.* **57**, 9–21.

Begin Z. B., Ehrlich A. and Nathan Y. (1974) Lake Lisan: the Pleistocene precursor of the Dead Sea. *Geol. Surv. Isr. Bull.* **63**, 1–30.

Begin Z. B., Stein M., Katz A., Machlus M., Rosenfeld A., Buchbinder B. and Bartov Y. (2004) Southward migration of rain tracks during the last glacial, revealed by salinity gradient in Lake Lisan (Dead Sea rift). *Quat. Sci. Rev.* **23**, 1627–1636.

Bookman (Ken-Tor) R., Enzel Y., Agnon A. and Stein M. (2004) Late Holocene lake levels of the Dead Sea. *Geo. Soc. Am. Bull.* **116**, 555–571.

Canfield D. E. (2001) Isotope fractionation by natural populations of sulfate-reducing bacteria. *Geochim. Cosmochim. Acta* **65**, 1117–1124.

Chambers L. A., Trudinger P. A., Smith J. W. and Burns M. S. (1975) Fractionation of sulfur isotopes by continuous cultures of Desulfivibrio Desulfuricans. *Can. J. Microbiol.* **21**, 1602–1607.

Coleman M. L. and Moore M. P. (1978) Direct reduction of sulfate to sulfur dioxide for isotopic analysis. *Anal. Chem.* **50**, 1594–1595.

Enzel Y., Bookman (Ken-Tor) R., Sharon D., Gvirtzman H., Dayan U., Ziv B. and Stein M. (2003) Late Holocene climates of the Near East deduced from Dead Sea level variations and modern regional winter rainfall. *Quat. Res.* **60**, 263–273.

Eugster H. P. (1970) Chemistry and origin of the brines of Lake Magadi, Kenya. *Spec. Publ. Min. Soc. Am.* **3**, 215–235.

Eugster H. P. and Jones B. F. (1979) Behavior of major solutes during closed-basin brine evolution. *Am. J. Sci.* **279**, 609–631.

Eugster H. P. and Maglione G. (1979) Brines and evaporites of the Lake Chad basin, Africa. *Geochim. Cosmochim. Acta* **43**, 973–981.

Fry B., Cox J., Gest H. and Hayes J. M. (1986) Discrimination between S-34 and S-32 during bacterial metabolism of inorganic sulfur-compounds. *J. Bacteriol.* **165**, 328–330.

Fry B., Gest H. and Hayes J. M. (1988) S-34/S-32 fractionation in sulfur cycles catalyzed by anaerobic-bacteria. *Appl. Environm. Microbiol.* **54**, 250–256.

Gavrieli I. and Stein M. (2006). On the origin and fate of the brines in the Dead Sea basin. In *New Frontiers in Dead Sea Paleoenvironmental Research* (eds. Y. Enzel, A. Agnon and M. Stein). GSA Special Paper 401, pp. 183–194.

Gavrieli I., Yechieli Y., Halicz L., Spiro B., Bein A. and Efron D. (2001) The sulfur system in anoxic subsurface brines and its implication in brine evolutionary pathways: the Ca-chloride brines in the Dead Sea area. *Earth Planet. Sci. Lett.* **186**, 199–213.

Giessemann A., Jager H. J., Norman A. L., Krouse H. R. and Brand W. A. (1994) On-line sulfur-isotope determination using an elemental analyzer coupled to a mass spectrometer. *Anal. Chem.* **66**, 2816–2819.

Glennie K. W. and Buller A. T. (1983) The Permian Weissliegend of NW Europe: the partial deformation of eolian sands caused by the Zechstein transgression. *Sed. Geol.* **35**, 43–81.

Goldschmidt M. J., Arad A. and Neev D. (1967) The mechanism of the saline springs in the Lake Tiberias depression. *Geol. Surv. Isr. Bull.* **45**, 1–19.

Gvirtzman H. (2006) Groundwater hydrology and paleohydrology of the Dead Sea rift valley. In *New Frontiers in Dead Sea Paleoenvironmental Research* (eds. Y. Enzel, A. Agnon and M. Stein). GSA Special Paper 401, pp. 95–111.

Gvirtzman H. and Stanislavsky E. (2000) Paleohydrology of hydrocarbon maturation, migration and accumulation in the Dead Sea Rift. *Basin Res.* **12**, 79–93.

Gvirtzman H., Garven G. and Gvirtzman G. (1997) Thermal anomalies associated with forced and free ground-water convection in the Dead Sea rift valley. *GSA Bull.* **109**, 1167–1176.

Haase-Schramm A., Goldstein S. L. and Stein M. (2004) U–Th dating of Lake Lisan (late Pleistocene Dead Sea) aragonite and implications for glacial East Mediterranean climate change. *Geochim. Cosmochim. Acta* **68**, 985–1005.

Habicht K. S., Canfield D. E. and Rethmeier J. (1998) Sulfur isotope fractionation during bacterial reduction and disproportionation of thiosulfate and sulfide. *Geochim. Cosmochim. Acta* **62**, 2585–2595.

Habicht K. S. and Canfield D. E. (1996) Sulfur isotope fractionation in modern microbial mats and the evolution of the sulfur cycle. *Nature* **382**, 342–343.

Haliva A., Starinsky A. and Stein M. (2003) Mineralogy, petrography and $^{87}Sr/^{86}Sr$ ratios of fine-grain detrital sediments of the Dead Sea group: origin and means of transportation. *Isr. Geol. Soc. Annu. Meet.*, 49.

Hall J. K. (1997) Topography and bathymetry of the Dead Sea depression. In *The Dead Sea—The Lake and its Setting, Oxford Monographs on Geology and Geophysics* (eds. T.M. Niemi, Z. Ben-Avraham and J.R.). Vol. 36, pp. 11–21.

Hardie L. A. and Eugster H. P. (1970) The evolution of closed-basin brines. *Spec. Publ. Min. Soc. Am.* **3**, 273–290.

Hsu K. J., Montadert L., Bernoulli D., Cita M. B., Erickson A., Garrison R. E., Kidd R. B., Melieres F., Muller C. and Wright R. (1977) History of the Mediterranean salinity crisis. *Nature* **267**, 399–403.

Hurwitz S., Stanislavsky E., Lyakhovsky V. and Gvirtzman H. (2000) Transient groundwater–lake interactions in a continental rift: Sea of Galilee, Israel. *GSA Bull.* **112**, 1694–1702.

Kaplan I. R. and Rittenberg S. C. (1964) Microbiological fractionation of sulfur isotopes. *J. Gen. Microbiol.* **34**, 195–212.

Katz A. and Kolodny N. (1989) Hypersaline brine diagenesis and evolution in the Dead-Sea Lake Lisan system (Israel). *Geochim. Cosmochim. Acta* **53**, 59–67.

Katz A., Kolodny Y. and Nissenbaum A. (1977) The geochemical evolution of the Pleistocene Lake Lisan-Dead Sea system. *Geochim. Cosmochim. Acta* **41**, 1609–1626.

Katz A., Starinsky A., Taitel-Goldman N. and Beyth M. (1981) Solubilities of gypsum and halite in the Dead Sea and its mixture with seawater. *Limnol. Oceanogr.* **26**, 709–716.

Kaufman A. (1971) U-series dating of Dead Sea basin carbonates. *Geochim. Cosmochim. Acta* **35**, 1269–1281.

Kemp A. L. W. and Thode H. G. (1968) The mechanism of the bacterial reduction of sulfate and sulfite from isotope fractionation studies. *Geochim. Cosmochim. Acta* **32**, 71–91.

Kendall A. C. (1992) Evaporites. In *Facies Models: Responses to Sea Level Change, Geolog. Ass. Canada* (ed. N. P. James). pp. 375–409.

Kolodny Y., Stein M. and Machlus M. (2005) Sea–Rain–Lake relation in the last Glacial East Mediterranean revealed by $\delta^{18}O$–$\delta^{13}C$ in Lake Lisan aragonites. *Geochim. Cosmochim. Acta* **69**, 4045–4060.

Krijgsman W., Hilgen F. J., Raffi I., Sierro F. J. and Wilson D. S. (1999) Chronology, causes and progression of the Messinian salinity crisis. *Nature* **400**, 652–655.

Krumgalz B. S. and Millero F. J. (1983) Physio-chemical study of the Dead Sea waters III. On gypsum saturation in Dead Sea waters and their mixture with Mediterranean water. *Mar. Chem.* **13**, 127–139.

Laronne Ben-Itzhak L. and Gvirtzman H. (2005) Groundwater flow along and across structural folding: an example from the Judean Desert, Israel. *J. Hydrol.* **312**, 51–69.

Machlus M., Enzel Y., Goldstein S. L., Marco S. and Stein M. (2000) Reconstructing low levels of Lake Lisan by correlating fan-delta and lacustrine deposits. *Quat. Int.*(73/74), 137–144.

Magee J. W., Bowler J. M., Miller G. H. and Williams D. L. G. (1995) Stratigraphy, sedimentology, chronology and palaeohydrology of Quaternary lacustrine deposits at Madigan Gulf, Lake Eyre, south Australia. *Palaeo. Palaeo. Palaeo.* **113**, 3–42.

Migowski C., Stein M., Prasad S., Negendank J. F. W. and Agnon A. (2006) Holocene climate variability and cultural evolution in the Near East from the Dead Sea sedimentary record. *Quat. Res.* **66**, 421–431.

Migowski C., Agnon A., Bookman R., Negendank J. F. W. and Stein M. (2004) Recurrence pattern of Holocene earthquakes along the Dead Sea transform revealed by varve-counting and radiocarbon dating of lacustrine sediments. *Earth Planet. Sci. Lett.* **222**, 301–314.

Neev D. and Emery K. O. (1967) The Dead Sea: depositional processes and environments of evaporites. *Geol. Surv. Isr. Bull.* **41**, 1–147.

Nissenbaum A. and Kaplan I. (1976) Sulfur and carbon isotopic evidence for biogeochemical processes in the Dead Sea ecosystem. In *Environmental Biogeochemistry* (ed. J. Nriagu). Ann Arbor Science Publishers, pp. 309–325.

Oren A., Gavrieli I., Gavrieli J., Kohen M., Lati J. and Aharoni M. (2004) Biological effects of dilution of Dead Sea brine with seawater: implications for the planning of the Red Sea–Dead Sea "Peace conduit". *J. Mar. Sys.* **46**, 121–131.

Parkhurst D. L. and Appelo C. A. J. (1999) User's guide to PHREEQC (version 2)—a computer program for speciation, batch-reaction, one-dimensional, transport, and inverse-geochemical calculations: USGS Water-Resources Investigations Report 99-4259, 310 p.

Prasad S., Vos H., Negendank J. F. W., Waldmann N., Goldstein S. L. and Stein M. (2004) Evidence from Lake Lisan of solar influence on decadal- to centennial-scale climate variability during marine oxygen isotope stage 2. *Geology* **32**, 581–584.

Raab M., Friedman G. M., Spiro B., Starinsky A. and Zak I. (2000) The geological history of Pliocene–Pleistocene evaporites in Mount Sedom (Israel) and how strontium and sulfur isotopes relate to their origin. *Carbonates and Evaporites* **15**, 93–114.

Raab M., Friedman G. M., Spiro B., Starinsky A. and Zak I. (1997) The geological history of Messinian (Upper Miocene) evaporites in the central Jordan Valley (Israel) and how strontium and sulfur isotopes relate to their origin. *Carbonates and Evaporites* **12**, 296–324.

Rouchy J. M. and Caruso A. (2006) The Messinian salinity crisis in the Mediterranean basin: a reassessment of the data and an integrated scenario. *Sed. Geol.* **188–189**, 35–67.

Ron H., Nowaczyk N. R., Frank U., Marco S. and McWilliams M. O. (2006) Magnetic properties of Lake Lisan and Holocene Dead Sea sediments and the fidelity of chemical and detrital remanent magnetization. In *New Frontiers in Dead Sea Paleoenvironmental Research* (eds. Y. Enzel, A. Agnon and M. Stein). GSA Special Paper 401, pp. 171–182.

Spencer R. J., Eugster H. P. and Jones B. F. (1985) Geochemistry of great Salt Lake, Utah II: Pleistocene–Holocene evolution. *Geochim. Cosmochim. Acta* **49**, 739–747.

Stanislavsky E. and Gvirtzman H. (1999) Basin-scale migration of continental-rift brines: paleohydrologic modeling of the Dead Sea Basin. *Geology* **27**, 791–794.

Starinsky A. (1974) Relationship between Ca-chloride brines and sedimentary rocks in Israel. Ph.D., Hebrew University (in Hebrew, Engl. abstract).

Stein M. (2001) The sedimentary and geochemical record of Neogene-Quaternary water bodies in the Dead Sea Basin—inferences for the regional paleoclimatic history. *J. Paleolimn.* **26**, 271–282.

Stein M., Agnon A., Katz A. and Starinsky A. (2002) Strontium isotopes in discordant dolomite bodies of the Judea Group, Dead Sea basin. *Isr. Jr. Earth Sci.* **51**, 219–224.

Stein M., Starinsky A., Agnon A., Katz A., Raab M., Spiro B. and Zak I. (2000) The impact of brine–rock interaction during marine evaporite formation on the isotopic Sr record in the oceans: evidence from Mt. Sedom, Israel. *Geochim. Cosmochim. Acta* **64**, 2039–2053.

Stein M., Starinsky A., Katz A., Goldstein S. L., Machlus M. and Schramm A. (1997) Strontium isotopic, chemical, and sedimentological evidence for the evolution of Lake Lisan and the Dead Sea. *Geochim. Cosmochim. Acta* **61**, 3975–3992.

Torfstein A., Haase-Schramm A., Waldmann N., Kolodny Y. and Stein M. (2007) U–Th, $\delta^{18}O$ and paleomagnetic dating of a mid-Pleistocene lacustrine sequence: the Amora Formation, Mount Sedom, Israel. *Geochim. Cosmochim. Acta* **71**, A1031.

Torfstein A., Gavrieli I. and Stein M. (2005) The sources and evolution of sulfur in the saline Lake Lisan (paleo-Dead Sea). *Earth Planet. Sci. Lett.* **236**, 61–77.

Waldmann N., Starinsky A. and Stein M. (2007) Primary carbonates and Ca-chloride brines as monitors of the paleo-hydrological regime in the Dead Sea basin. *Quat. Sci. Rev.* **26**, 2219–2228.

Warren J. K. (1989) *Evaporite sedimentology*. Prentice Hall Advanced Reference Series, pp. 285.

Yechieli Y. (2006) Response of the groundwater system to changes in the Dead Sea level. *In New Frontiers in Dead Sea Paleoenvironmental Research* (eds. Y. Enzel, A. Agnon and M. Stein). GSA Special Paper 401, pp. 113–126.

Yechieli Y. (2000) Fresh-saline ground water interface in the Western Dead Sea area. *Groundwater* **38**, 615–623.

Zak I. (1967) The Geology of Mt. Sedom. Ph.D., Hebrew University (in Hebrew, Engl. Abstract).

Associate editor: Martin B. Goldhaber